6. H. Ishii *et al.*, *Nature* **426**, 540 (2003).
7. S. M. Bachilo *et al.*, *Science* **298**, 2361 (2002).
8. M. J. O'Connell *et al.*, *Science* **297**, 593 (2002).
9. M. Y. Sfeir *et al.*, *Science* **306**, 1540 (2004).
10. J. A. Misewich *et al.*, *Science* **300**, 783 (2003).
11. M. Freitag, Y. Martin, J. A. Misewich, R. Martel, Ph. Avouris, *Nano Lett.* **3**, 1067 (2003).
12. T. Ando, *J. Phys. Soc. Jpn.* **66**, 1066 (1997).
13. T. G. Pedersen, *Phys. Rev. B* **67**, art. no. 073401 (2003).
14. V. Perebeinos, J. Tersoff, Ph. Avouris, *Phys. Rev. Lett.* **92**, art. no. 257402 (2004).
15. C. D. Spataru, S. Ismail-Beigi, L. X. Benedict, S. G. Louie, *Phys. Rev. Lett.* **92**, art. no. 077402 (2004).
16. E. Chang, G. Bussi, A. Ruini, E. Molinari, *Phys. Rev. Lett.* **92**, art. no. 196401 (2004).
17. C. L. Kane, E. J. Mele, *Phys. Rev. Lett.* **90**, art. no. 207401 (2003).
18. H. B. Zhao, S. Mazumdar, *Phys. Rev. Lett.* **93**, art. no. 157402 (2004).
19. H. Htoon, M. J. O'Connell, P. J. Cox, S. K. Doorn, V. I. Klimov, *Phys. Rev. Lett.* **93**, art. no. 027401 (2004).
20. Y. Z. Ma *et al.*, *J. Chem. Phys.* **120**, 3368 (2004).
21. R. Saito, G. Dresselhaus, M. S. Dresselhaus, *Physical Properties of Carbon Nanotubes* (Imperial College Press, London, 1998).
22. A. Hagen, T. Hertel, *Nano Lett.* **3**, 383 (2003).
23. M. S. Dresselhaus, G. Dresselhaus, A. Jorio, *Annu. Rev. Mater. Res.* **34**, 247 (2004).
24. R. Farchioni, G. Grosso, Eds., *Organic Electronic Materials: Conjugated Polymers and Low Molecular Weight Organic Solids* (Springer, Berlin, 2001).
25. P. R. Callis, *Annu. Rev. Phys. Chem.* **48**, 271 (1997).
26. Y. R. Shen, *The Principles of Nonlinear Optics* (Wiley, New York, 1984).
27. T. Ogawa, T. Takagahara, *Phys. Rev. B* **44**, 8138 (1991).
28. A. Shimizu, T. Ogawa, H. Sakaki, *Phys. Rev. B* **45**, 11338 (1992).
29. G. Dukovic *et al.*, *J. Am. Chem. Soc.* **126**, 15269 (2004).
30. To eliminate the influence of background in determining the two-photon excitation spectrum of SWNTs of a given chiral index, we plotted the experimental emission spectra, corresponding to vertical cuts in the two-dimension contour plot of Fig. 2, for a series of two-photon excitation energies. We then fit each emission spectrum to a sum of Lorentzian features corresponding to the relevant nanotube species in our ensemble sample. The two-photon excitation spectrum for a given nanotube chiral index was then obtained by tracking the peak height of corresponding fluorescence contribution as a function of the two-photon excitation energy.
31. For the continuum states in a 1D direct-gap material, the two-photon absorption cross section σ_{TPA} scales as $\sigma_{TPA} \propto (E - E_g)^{1/2}$ within the free carrier picture, where E denotes the photon energy and E_g the bandgap energy. This form is modified by strong electron-hole interactions. Within the Wentzel-Kramers-Brillouin approximation, one can show generally that this correction leads to an enhancement near the band edge that produces a step function for the two-photon cross-section, $\sigma_{TPA} \propto \theta(E - E_g)$, where θ is the usual Heavyside function. This correction is analogous to the well-known result for one-photon excitonic transitions in bulk semiconductors (*32*).
32. R. J. Elliott, *Phys. Rev.* **108**, 1384 (1957).

33. We would like to thank Ph. Avouris, M. Hybertsen, M. Loy, P. Kim, V. Perebeinos, and M. Sfeir for helpful discussions. Supported by the Nanoscale Science and Engineering Initiative of the NSF (grant no. CHE-0117752), by the New York State Office of Science, Technology, and Academic Research, and by the U.S. Department of Energy Office of Basic Energy Sciences (grant nos. DOE-FG02-98ER14861 and DE-FG02-03ER15463).

26 January 2005; accepted 14 March 2005
10.1126/science.1110265

Zircon Thermometer Reveals Minimum Melting Conditions on Earliest Earth

E. B. Watson[1]* and T. M. Harrison[2,3]

Ancient zircons from Western Australia's Jack Hills preserve a record of conditions that prevailed on Earth not long after its formation. Widely considered to have been a uniquely violent period geodynamically, the Hadean Eon [4.5 to 4.0 billion years ago (Ga)] has recently been interpreted by some as far more benign—possibly even characterized by oceans like those of the present day. Knowledge of the crystallization temperatures of the Hadean zircons is key to this debate. A thermometer based on titanium content revealed that these zircons cluster strongly at ~700°C, which is indistinguishable from temperatures of granitoid zircon growth today and strongly suggests a regulated mechanism producing zircon-bearing rocks during the Hadean. The temperatures substantiate the existence of wet, minimum-melting conditions within 200 million years of solar system formation. They further suggest that Earth had settled into a pattern of crust formation, erosion, and sediment recycling as early as 4.35 Ga.

The first 500 million years of Earth evolution, a period known as the Hadean Eon, was the most geodynamically vigorous in our planet's history. During this time, it is variously speculated that the Earth may have experienced collision with a Mars-sized object (*1*), formed a global magma ocean (*2*), grown the first continents (*3*), and seen the emergence of life (*4*). It is also entirely possible, and consistent with the geochemical record, that none of these events took place. The fundamental problem is that we have no rock record from this interval to learn about these processes because the oldest firmly dated rock is 4.04 Ga (*5*). How, then, are we to gain further insights into the formative stages of Earth evolution?

Although no Hadean rocks are yet documented, we are not entirely without a geochemical record of the period between 4.5 and 4.0 Ga. The existence of zircons >4.1 Ga preserved in Early Archean metasediments at Mt. Narryer and Jack Hills, Western Australia, has been known for more than 20 years (*6*, *7*), and recent measurements have begun to glean information from them regarding the nature of the Hadean Earth. For example, Hf isotopic studies suggest the existence of reworked continental crust before 4.1 Ga (*8*). Oxygen isotope results have been interpreted as indicating that protoliths of ~4.3-Ga magmas formed in the presence of water at the Earth's surface (*9*, *10*). Xenon isotopic studies of these ancient zircons have permitted an estimate of the initial terrestrial plutonium/uranium ratio, a parameter key to understanding the origin and evolution of the atmosphere (*11*).

These and other results have challenged the traditional view that continental formation and development of a hydrosphere were frustrated by meteorite bombardment and basaltic igneous activity until ~4 Ga. Instead, they suggest a surface environment and petrogenetic processes much more similar to those of the present day. Here, we exploit a newly developed thermometer, based on Ti incorporation into crystallizing zircon, to assess the nature of Hadean magmatism. From these analyses, we conclude that Jack Hills zircons were dominantly sourced from crustal melts that formed at temperatures ranging from those characteristic of wet, minimum melting to vapor absent melting under anatectic conditions.

Titanium content is uniquely suitable as a potential indicator of zircon crystallization temperature. As a tetravalent ion under all relevant geologic conditions, Ti enters the zircon lattice in homovalent replacement of Zr^{4+} or Si^{4+}. Consequently, Ti uptake does not depend on the availability of other charge-compensating ions. For the TiO_2-saturated case (i.e., rutile present in the system), the thermodynamic basis of the thermometer is the simple reaction

$$TiO_{2(\text{rutile})} = TiO_{2(\text{zircon})} \qquad (1)$$

for which the equilibrium constant is

$$k_1 = \frac{a_{TiO_2}^{\text{zircon}}}{a_{TiO_2}^{\text{rutile}}}$$

where a_{TiO_2} is the activity of TiO_2 in rutile or zircon as indicated by the superscript. Because rutile is nearly pure TiO_2, $a_{TiO_2}^{\text{rutile}} \sim 1$, so

[1]Department of Earth and Environmental Sciences, Rensselaer Polytechnic Institute, Troy, NY 12180, USA. [2]Research School of Earth Sciences, Australian National University, Canberra, ACT 2601, Australia. [3]Department of Earth and Space Sciences and Institute of Geophysics and Planetary Physics, University of California, Los Angeles, CA 90095, USA.

*To whom correspondence should be addressed. E-mail: watsoe@rpi.edu

$k \cong a_{TiO_2}^{zircon}$. Therefore

$$a_{TiO_2}^{zircon} = \gamma_{TiO_2}^{zircon} \cdot X_{TiO_2}^{zircon} = \exp\frac{-\Delta G_1^o}{RT} \quad (2)$$

where γ is the activity coefficient and X the mole fraction of TiO_2 in zircon, ΔG_1^o is the standard-state free-energy change for reaction 1, R is the gas constant, and T is absolute temperature. Assuming $\gamma_{TiO_2}^{zircon}$ is constant, the logarithm of the Ti concentration in zircon is expected to be linear in T^{-1}. Confirmation and quantification of this relation would constitute a crystallization thermometer for zircon in the presence of rutile.

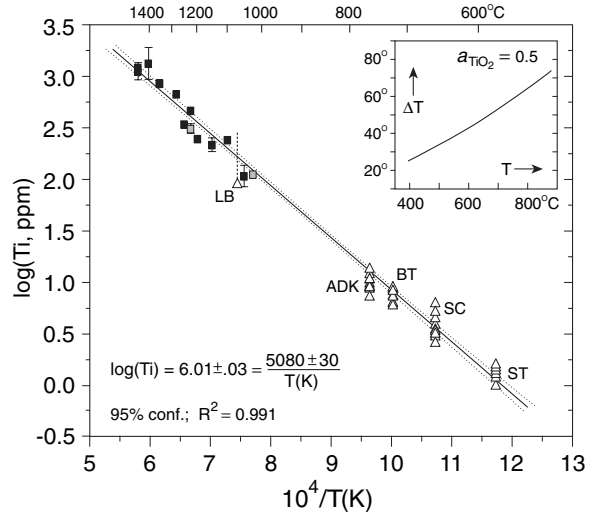

Fig. 1. Temperature dependence of Ti incorporation into synthetic zircons (black and gray squares are at 1 and 2 GPa, respectively) and zircons separated from natural rocks (triangles). The natural samples are Bishop Tuff (BT) (*13*), Adirondack migmatite (ADK) (*14*), Stillup Tal aluminous schist (ST) (*15*), Labait harzburgite (LB) (*16*), and Santa Catalina migmatite (SC) (*17*). All systems contain rutile except BT, which contains ilmenite (see text). For the natural zircons analyzed by ion microprobe (ADK, BT, SC, and ST), individual analyses rather than mean values are plotted. The variation in Ti content of zircons from a specific rock is well outside the analytical uncertainty (*23*) and thus may reflect real variation in growth temperature (the ion microprobe lacks the spatial resolution to systematically traverse a zircon rim). The data are plotted at the temperatures estimated from other thermometers (or at the midpoint when a range is indicated). In the LB case, the triangle represents the mean of ~90 spot analyses in the interiors of two zircons; the Ti content is higher in patches near the margins of these zircons, as indicated by the dotted line extending upward from the plotted symbol. Pyroxene thermometry places the temperature of the host at 1070°C (*37*), but a brief, late heating event is recorded by the pyroxene rim compositions. The uncertainty in the best-fit line is indicated in the figure; this translates into an uncertainty of ±10°C (2σ) at relevant application temperatures. The inset illustrates the extent to which the Ti content of zircons would underestimate temperature (by ΔT) if the activity of TiO_2 in the system were 0.5.

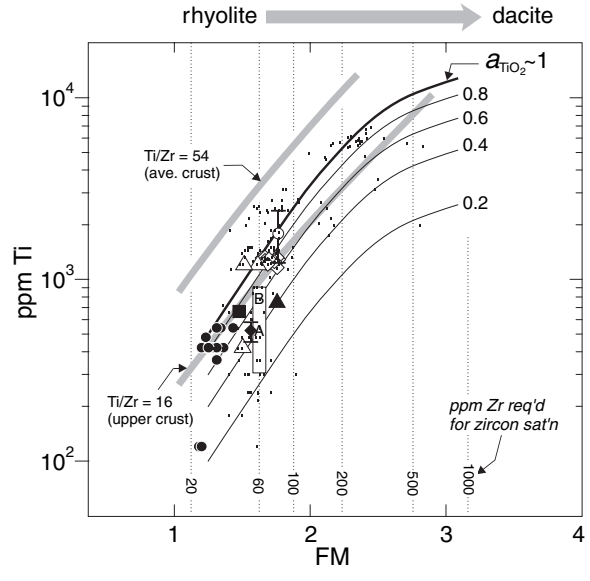

Fig. 2. Analyses of silicic glass inclusions and volcanic glasses in relation to estimated TiO_2 activity in magmatic melts based on the rutile saturation model of Ryerson and Watson (*20*) for 0.1-GPa pressure. The heavy black curve labeled "$a_{TiO_2} \sim 1$" delineates Ti concentrations sufficient for rutile saturation according to the Ryerson-Watson (R-W) model (fig. S1); curves for $a_{TiO_2} < 1$ were calculated assuming Henrian behavior in the melt. The vertical dotted lines indicate the approximate amount of Zr required for zircon crystallization at a given value of FM and implied T (*21*). The diagram reveals that most natural melts capable of crystallizing zircon also have TiO_2 activities exceeding ~0.5. Because the $a_{TiO_2} \sim 1$ curve corresponds to a Ti/Zr ratio at rutile and zircon cosaturation of ~20—compared with a value of ~50 for the average crust (*38*)—most terrestrial melts will saturate in a Ti phase before zircon. The activity curves are approximate because the R-W model is based principally on melts having FM > 3; however, these curves are broadly consistent with the locations of peraluminous melt inclusions containing ilmenite (●) (*39*), and with the independently calculated a_{TiO_2} value of ~0.6 for the Bishop Tuff ("B") and ~0.4 for the Bandelier rhyolite ("A") (*18*). Other symbols: (■) melt inclusion (MI) mean, Taylor Creek rhyolite (*40*); (▲) MI mean, Alid volcanic center, Eritrea (*41*); (♦) MI mean, Paleozoic volcanic ash (*42*); (◊) mean of MI in quartz, Ordovician bentonites, New York (*43*); (△) MI in Yellowstone rhyolites (*44*); (○) MI mean, Taupo, New Zealand (*45*); vertical white bar indicates the Ti range for MI in phenocrysts from Bishop Tuff (*46*) and Bandelier rhyolite (*47*). Other volcanic glasses and MI are plotted as black specks because Ti was analyzed as part of a major-element electron microprobe routine and the values have significant uncertainty [data sources (*48–50*); lowest SiO_2 contents are ~65 weight %].

The Ti thermometer was calibrated experimentally at 1025° to 1450°C (1 to 2 GPa) and by analysis of natural zircons known to have crystallized at ~580° to 1070°C on the basis of independent geothermometers. We used a piston-cylinder apparatus to grow zircons in the presence of rutile, both from aqueous solution and by crystallization from silicate melt (*12*). The Ti concentrations in these synthetic zircons were determined by electron microprobe analysis and range between ~100 parts per million (ppm) (1025°C) and ~1300 ppm (1450°C). The natural zircons were separated from five well-characterized rocks: the Bishop Tuff (*13*); a rutile-bearing migmatite from the Adirondack Mountains (*14*); a rutile-bearing aluminous schist from the Tauern Window in the Eastern Alps [Stillup Tal (*15*)]; a rutile-bearing metasomatic vein in a harzburgite nodule from Labait volcano in Tanzania (*16*); and a rutile-bearing migmatite from a mafic subduction complex exposed at Santa Catalina Island, California (*17*). Cathodoluminescence (CL) imaging confirmed a simple crystallization history for the Bishop Tuff (BT) zircons; those from the Adirondack migmatite (ADK), the Alpine schist (ST), and the California migmatite (SC) have inherited cores with CL-dark overgrowth rims of varying width believed to have formed at or near peak metamorphic conditions. Zircons in the Labait harzburgite (LB) are large euhedra (up to 500 μm) with CL zoning ranging from concentric to patchy. We determined Ti concentrations in these zircons (or rims) using an ion microprobe (see below) for the ADK, SC, ST, and BT cases and an electron microprobe for the more Ti-rich LB case. Analyses of ADK, SC, ST, and LB zircons are used directly in the calibration because rutile is present in the host rocks. In the BT case, however, the measured Ti contents of the zircons were adjusted upward slightly, in accordance with the subunity TiO_2 activity in the system, estimated to be 0.6 from the Ti contents of abundant quartz phenocrysts cocrystallized with the zircons (*18*) (note that the BT does contain ilmenite). The overall thermometer calibration (Fig. 1) conforms well to prediction (Eq. 2), spans almost 900°C in temperature, and shows little sensitivity to pressure. Application of this thermometer to zircons of unknown crystallization temperature requires simple measurement of Ti content.

Strictly speaking, the Ti-in-zircon thermometer applies to systems containing rutile. Accordingly, the temperatures measured must be regarded as minimum values unless cocrystallization with rutile can be established. This

consideration is important for the Hadean zircons because they are removed from their original surroundings and their coexistence with rutile is generally uncertain. Fortunately, this does not appreciably weaken the constraint on zircon growth temperature provided by Ti content, for the following reasons. In metamorphic systems, a_{TiO_2} ranges from 0.6 in metabasites to ~1 in metapelites (*19*). In igneous systems, a_{TiO_2} is also broadly constrained by existing knowledge of the rutile saturation surface (*20*). For a wide variety of magmatic melts, the same factors that lead to high activities of ZrO_2 (resulting in zircon saturation) (*21*) also lead to high activities of TiO_2. Saturation in zircon and rutile depend weakly on pressure and strongly on temperature and melt composition, where the latter is expressed as a ratio of cation fractions: $FM = (Na^+ + K^+ + 2R^{2+})/(Al^{3+} \cdot Si^{4+})$, where R = Ca for the case of zircon (*21*) and R = Ca + Fe + Mg for rutile (*20*). If the Hadean zircons are magmatic, as is clearly the case for those with oscillatory zoning (see below), the range of possible host-melt compositions and temperatures is quite restricted—by virtue of the presence of zircon—for plausible levels of dissolved Zr. Broadly speaking, the limitations on melt composition and temperature imposed by the presence of zircon itself restrict a_{TiO_2} to values generally >0.5 (Fig. 2). Only peralkaline melts are exempt from this general reasoning, because of the high solubilities of zircon (*22*) and the lack of systematic data on rutile solubility.

In summary, for most igneous and metamorphic rocks in existence today, a_{TiO_2} is 0.5 or higher. The host materials of the Hadean zircons cannot be assumed a priori to resemble those typical of more recent times, but their characteristics were governed by the same thermodynamic considerations. Given that a_{TiO_2} generally is ≥0.5, the crystallization temperatures of most of these zircons will not be underestimated by more than 50° to 60°C (Fig. 1, inset).

Using an ion microprobe (*23*), we measured Ti concentrations in 54 Jack Hills concordant zircons ranging in U-Pb age from 4.0 to 4.35 Ga. At least one analysis spot on each zircon was chosen to coincide with the locations where the ages were determined. Calculated temperatures from 69 spots range from 801° to 644°C (696° ± 33°C) (Fig. 3). In most cases, duplicate Ti determinations on single zircons yielded similar temperatures; however, one zircon fragment with CL zoning suggesting a simple magmatic history shows a systematic diminution in crystallization temperature from 778°C near the core to 751°C near the rim (Fig. 4). This pattern is consistent with progressive zircon growth during cooling of the host magma.

The most notable feature of these results is the low and restricted range of temperatures which, taken at face value, implies water-saturated melting conditions. Before we explore this possibility, we first examine two alternative scenarios. First, could the zircon temperature distribution result from cooling of melts derived from the expected high flux of impacting bolides? We rule out this possibility for the following reasons: (i) The melting temperature in the Qz-Ab-Or-H_2O system, even in the presence of the 270-bar steam atmosphere resulting from complete evaporation of the ocean (*24*), exceeds 800°C (*25*); (ii) the dispersion of the temperature distribution is low (Fig. 3), implying a dominant, regulated melting mechanism (this is especially true if the eight outliers in the distribution at $T > 750$°C are attributed to an alternative mechanism); and (iii) zircon saturation temperatures calculated for magmas produced by wholesale melting of average crust (*26*) exceed the average Hadean zircon temperatures we observe. Second, could the Hadean zircon temperature distribution reflect residual liquids that might have fractionated from higher temperature, mafic magmas? We believe this scenario is ruled out by the expectation that late-stage crystallization in a mafic complex would yield appreciably higher average temperatures for zircon formation. For example, calculated zircon saturation temperatures for late differentiates of the Skaergaard intrusion yield an average temperature of 870°C (*27*, *28*). Our thermometer gave temperatures of 787° to 806°C for three Skaergaard zircons analyzed in this study (these are probably biased downward slightly by undersaturation of the system in rutile). Moreover, although fractionation of mafic magma can indeed yield felsic melts and intermediate-temperature zircons, this mechanism does not seem to meet the requirement of a regulated mechanism suggested by our data.

Thus, we believe that our crystallization temperatures for the Hadean zircons provide definitive evidence about the state of the early Earth, especially when considered in the context of the inclusion assemblage documented by other workers. Minerals contained within Hadean zircons include quartz, K-feldspar, chloritized biotite, chlorite, amphibole, muscovite, albite, Ca-Al silicate (plagioclase), rutile, apatite, FeOOH, Ni-rich pyrite, thorite (ThO_2), and monazite (*29*, *30*). Collectively, these inclusions are characteristic of granitic assemblages or their hydrated and/or oxidized equivalents (*29*). Until now, the possibility has remained that the inclusion assemblage may represent siliceous, feldspathic material of an-

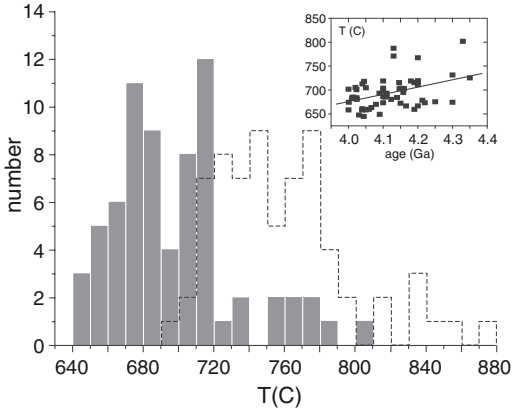

Fig. 3. Histogram of crystallization temperatures for Hadean zircons derived from measured Ti contents and thermometer calibration in Fig. 1. The distribution represented by the gray bars assumes $a_{TiO_2} = 1$; the dashed line shows the shift to somewhat higher temperatures for $a_{TiO_2} = 0.5$. The inset shows the distribution of zircon crystallization temperatures over time.

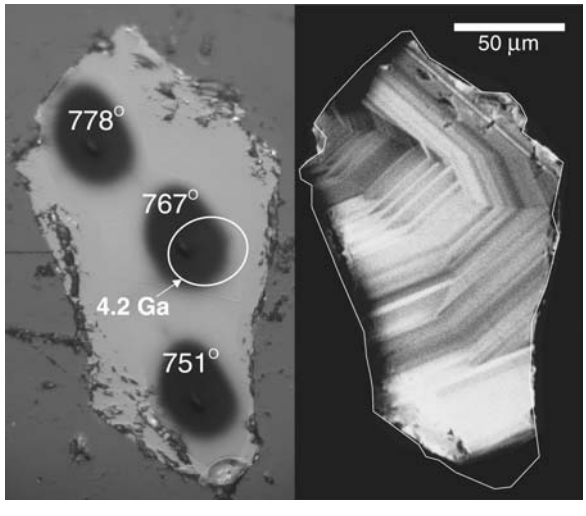

Fig. 4. (**Left**) Reflected-light image of Hadean zircon fragment ANU104-14.14, Au-coated for ion microprobe analysis. The white ellipse shows the location of the ion-microprobe analysis pit that yielded a concordant U-Pb age of 4.2 Ga. The dark spots reveal locations of ion-microprobe Ti analyses, from which temperatures were calculated using the information in Fig. 1. (**Right**) Cathodoluminescence image of the same zircon fragment, showing igneous growth zoning from core (top left) to rim (bottom); the thin white line is the fragment outline from the left photo. Note the correspondence of falling temperatures on the left with progressive growth on the right.

hydrous character that was altered by later exposure of the zircons to crustal metamorphic fluids. The temperatures measured by our Ti thermometer provide strong evidence against this possibility: Even with allowances for subunity TiO_2 activity (Fig. 2), they are simply too low for the zircons to have crystallized from dry siliceous melts (*31*). The restricted range of temperatures suggests, furthermore, that a highly reproducible set of circumstances removed melt fertility from rocks under prograde conditions consistent with crustal anatexis throughout the Hadean. Temperatures for zircons >4.2 Ga are sparse, but the present database hints at a slight down-temperature "focusing" of typical magmatic conditions between 4.35 and 4.0 Ga (Fig. 3, inset).

The simplest scenario is melting in an ensemble of crustal environments not unlike that of today under conditions at or close to water saturation. Taken collectively, our zircon crystallization temperatures mimic expectations for "modern-day" igneous zircons, with most pointing to a crustal anatectic origin.

The present results substantiate the existence of wet, minimum melting conditions at 4.35 to 4.0 Ga inferred from mineral inclusion studies and are consistent with the early Hadean hydrosphere hypothesis (*9*, *10*). They strongly suggest, moreover, that within ~100 million years of formation, Earth had settled into a pattern of crust formation, erosion, and sediment recycling similar to that produced during the known era of plate tectonics. The rapid establishment of this cycle implies, further, that the pace of geologic activity in general (driven by rapid mantle convection) was much faster in the Hadean than in more recent times.

References and Notes

1. W. Benz, W. L. Slattery, A. G. W. Cameron, *Icarus* **66**, 515 (1986).
2. K. Righter, M. J. Drake, *Earth Planet. Sci. Lett.* **171**, 383 (1999).
3. R. L. Armstrong, *Philos. Trans. R. Soc. London Ser. A* **301**, 443 (1981).
4. S. J. Mojzsis *et al.*, *Nature* **384**, 55 (1996).
5. S. A. Bowring, I. Williams, *Contrib. Mineral. Petrol.* **134**, 3 (1999).
6. D. O. Froude *et al.*, *Nature* **304**, 616 (1983).
7. W. Compston, R. T. Pidgeon, *Nature* **321**, 766 (1986).
8. Y. Amelin, D. C. Lee, A. N. Halliday, R. T. Pidgeon, *Nature* **399**, 252 (1999).
9. S. J. Mojzsis, T. M. Harrison, R. T. Pidgeon, *Nature* **409**, 178 (2001).
10. S. A. Wilde, J. W. Valley, W. H. Peck, C. M. Graham, *Nature* **409**, 175 (2001).
11. G. Turner, T. M. Harrison, G. Holland, S. J. Mojzsis, J. Gilmour, *Science* **306**, 89 (2004).
12. E. B. Watson, D. A. Wark, J. B. Thomas, in preparation.
13. B. T. Peppard, I. M. Steele, A. M. Davis, P. J. Wallace, A. T. Anderson, *Am. Mineral.* **86**, 1034 (2001).
14. L. Storm, F. S. Spear, *J. Metamorph. Geol.* **23**, 107 (2005).
15. J. Selverstone, G. Morteani, J.-M. Staude, *J. Metamorph. Geol.* **9**, 419 (1991).
16. R. L. Rudnick *et al.*, in *Proc. Seventh International Kimberlite Conference,* Cape Town, South Africa, J. J. Gurney, S. R. Richardson, Eds. (Red Barn, Cape Town, South Africa, 1999), pp. 728–735.
17. S. S. Sorensen, *J. Metamorph. Geol.* **6**, 405 (1988).
18. D. A. Wark, A. T. Anderson, E. B. Watson, *Eos Trans. AGU* (joint assembly program and abstracts, 2004).
19. E. D. Ghent, M. Z. Stout, *Contrib. Mineral. Petrol.* **86**, 248 (1984).
20. F. J. Ryerson, E. B. Watson, *Earth Planet. Sci. Lett.* **86**, 225 (1987).
21. E. B. Watson, T. M. Harrison, *Earth Planet. Sci. Lett.* **64**, 295 (1983).
22. E. B. Watson, *Contrib. Mineral. Petrol.* **70**, 407 (1979).
23. The ion microprobe analyses were performed at Woods Hole Oceanographic Institution using a Cameca ims 3f. A primary (O^-) ion-beam current of 5 nA was used in most cases, which resulted in a spot size of 15 to 20 μm. Four 30-s acquisition intervals at each spot resulted in a minimum detection limit (MDL) of ~0.1 ppm Ti using the relatively low-abundance isotope ^{49}Ti (5.5% of Ti). Titanium-48 (74% abundance) cannot be used for analysis of zircons with the ims 3f because of interfering $^{96}Zr^{2+}$ (2.8% isotopic abundance). For this reason, previously published values for Ti content of zircons (*32*, *33*) may be too high. The 2σ analytical uncertainty obtained with the ims 3f was ±20% and ±6%, respectively, at the 1- and 10-ppm levels (corresponding to temperatures of ~570° and ~740°C). The analytical error increases the ±10° uncertainty in the thermometer itself (Fig. 1) to ±16° at 570°C and ±11° at 740°C.
24. N. Sleep, K. Zahnle, *J. Geophys. Res.* **103**, 28,529 (1998).
25. F. Holtz, A. Becker, M. Freise, W. Johannes, *Contrib. Mineral. Petrol.* **141**, 347 (2001).
26. Calculated Zr saturation temperatures (*21*) for the 19,034 analyses in the OZCHEM National Whole Rock Geochemistry GIS Database (https://www.ga.gov.au/products; includes Australia, Papua New Guinea, Antarctica, Solomon Islands, and New Zealand) between 40 and 80% SiO_2 for which requisite data are available (*21*) yield a median of 780°C, with more than 80% of all calculated temperatures greater than the mean of our Hadean results (i.e., 696°C). If representative of the Hadean crustal average, then it is highly unlikely that the temperature distribution in Fig. 3 could reflect a limitation imposed by the Zr concentration of crustal rocks.
27. C. K. Brooks, *Geochim. Cosmochim. Acta* **33**, 357 (1969).
28. L. R. Wager, G. M. Brown, *Layered Igneous Rocks* (Oliver and Boyd, Edinburgh, 1968).
29. D. Trail, S. J. Mojzsis, T. M. Harrison, *Geochim. Cosmochim. Acta* **68**, A743 (2004).
30. R. Maas, P. D. Kinny, I. S. Williams, D. O. Froude, W. Compston, *Geochim. Cosmochim. Acta* **56**, 1281 (1992).
31. Water is required to depress the solidus to temperatures below ~960°C—the dry solidus of rocks of broadly granitic character (*34*–*36*).
32. E. A. Belousova, W. L. Griffin, S. Y. O'Reilly, N. I. Fisher, *Contrib. Mineral. Petrol.* **143**, 602 (2002).
33. P. W. O. Hoskin, *Geochim. Cosmochim. Acta* **69**, 637 (2005).
34. O. F. Tuttle, N. L. Bowen, *Geol. Soc. Am. Mem.* **74** (1958).
35. W. C. Luth, R. H. Jahns, O. F. Tuttle, *J. Geophys. Res.* **9**, 759 (1964).
36. J. A. Whitney, *J. Geol.* **83**, 1 (1975).
37. C.-T. Lee, R. L. Rudnick, in *Proc. Seventh International Kimberlite Conference,* Cape Town, South Africa, J. J. Gurney, S. R. Richardson, Eds. (Red Barn, Cape Town, South Africa, 1999), pp. 503–521.
38. S. R. Taylor, S. M. McLennan, *The Continental Crust: Its Composition and Evolution* (Blackwell Scientific, Oxford, 1985).
39. G. B. Morgan VI, D. London, R. G. Luedke, *J. Petrol.* **39**, 601 (1998).
40. J. D. Webster, W. A. Duffield, *Am. Mineral.* **76**, 1628 (1991).
41. J. B. Lowenstern, M. A. Clynne, T. B. Bullen, *J. Petrol.* **38**, 1707 (1997).
42. J. D. Webster, R. D. Congdon, P. C. Lyons, *Geochim. Cosmochim. Acta* **59**, 711 (1995).
43. B. Hanson, J. W. Delano, D. J. Lindstrom, *Am. Mineral.* **81**, 1249 (1996).
44. I. N. Bindeman, J. W. Valley, *J. Petrol.* **42**, 1491 (2001).
45. N. W. Dunbar, P. R. Kyle, *Am. Mineral.* **78**, 612 (1993).
46. N. W. Dunbar, R. L. Hervig, *J. Geophys. Res.* **97**, 15129 (1992).
47. N. W. Dunbar, R. L. Hervig, *J. Geophys. Res.* **97**, 15151 (1992).
48. C. L. Harford, R. S. J. Sparks, A. E. Fallick, *J. Petrol.* **44**, 1503 (2003).
49. P. E. Izbekov, J. C. Eichelberger, B. V. Ivanov, *J. Petrol.* **45**, 2325 (2004).
50. P. A. Cawood, E. C. Leitch, *Proc. Ocean Drill. Prog.* **156**, 343 (1997).

51. We thank E. Baxter, R. Rudnick, L. Storm, F. Spear, and D. Wark for providing rock samples and/or zircon separates for the thermometry calibration, and M. Hamilton for the Skaergaard zircons. We also thank G. Layne (ion microprobe), D. Wark, S. Mojzsis, P. Holden, E. Q. Reid, Z. Bruce, S. Mussett, and J. Thomas for scientific discussions and assistance with analytical aspects. The work was supported at Rensselaer Polytechnic Institute by NSF grants EAR 0073752 and EAR 0440228 (to E.B.W.), at Australian National University by Australian Research Council grant DP0342709 (to T.M.H.), and at the University of California, Los Angeles, by grants from the NSF Earth Sciences: Instrumentation and Facilities (EAR/IF) program and NASA's Exobiology program and National Astrobiology Institute.

Supporting Online Material

www.sciencemag.org/cgi/content/full/308/5723/841/DC1
Fig. S1

9 February 2005; accepted 14 March 2005
10.1126/science.1110873

An Octane-Fueled Solid Oxide Fuel Cell

Zhongliang Zhan and Scott A. Barnett*

There are substantial barriers to the introduction of hydrogen fuel cells for transportation, including the high cost of fuel-cell systems, the current lack of a hydrogen infrastructure, and the relatively low fuel efficiency when using hydrogen produced from hydrocarbons. Here, we describe a solid oxide fuel cell that combines a catalyst layer with a conventional anode, allowing internal reforming of *iso*-octane without coking and yielding stable power densities of 0.3 to 0.6 watts per square centimeter. This approach is potentially the basis of a simple low-cost system that can provide substantially higher fuel efficiency by using excess fuel-cell heat for the endothermic reforming reaction.

Improving fuel efficiency is one of the key reasons, along with reduced pollution, for the adoption of fuel cells for applications such as transportation. Improving efficiency not only reduces fuel consumption but also reduces the associated CO_2 emission. Although fuel cells can achieve efficiencies of 50 to 60%, overall "well-to-wheels" efficiencies are cur-